buildings

MDPI

Article

Investigation into the Early Cracking Behavior of High-Geothermal Tunnel Lining Concrete Based on Thermal–Mechanical Coupling Model

Si Xie [1], Dan Zhao [2], Peng Yi [3,4], Qian Chen [3,4] and Wei Liu [3,4,*]

[1] State Key Laboratory of Intelligent Geotechnics and Tunnelling, China Railway First Survey and Design Institute Group Co., Ltd., Xi'an 710043, China; rachelcsu@163.com
[2] Shenzhen Municipal Design and Research Institute Co., Ltd., Shenzhen 518029, China; zhaod@szmedi.com.cn
[3] State Key Laboratory of Intelligent Geotechnics and Tunnelling & National Engineering Research Center of Deep Shaft Construction, Shenzhen University, Shenzhen 518060, China; 2100471026@email.szu.edu.cn (P.Y.); 2100471034@email.szu.edu.cn (Q.C.)
[4] Guangdong Provincial Key Laboratory of Durability for Marine Civil Engineering, College of Civil and Transportation Engineering, Shenzhen University, Shenzhen 518060, China
* Correspondence: liuwei@szu.edu.cn

Abstract: As a typical extreme environment, a high-geothermal environment poses severe challenges to tunnel construction in western China. In this paper, a thermal–mechanical coupling model was formulated to evaluate the cracking behavior of lining under high-geothermal conditions, considering the early property evolution of concrete. This was further validated by field monitoring and analyzed by adjusting the relevant parameters. Results indicate that the higher cracking risk occurred on the external surface of the lining sidewall after 24 h of casting. With the increase in surrounding rock temperature, the duration of cracking risk in the lining was extended. When the surrounding rock temperature exceeded 68.7 °C, thermal insulation measures were required for the lining structure. Notably, superior thermal insulation was achieved by applying a sandwich structure of rigid polyurethane materials with a thickness of 20–60 mm. In terms of curing conditions, adopting formwork with a larger heat convection coefficient was conducive to reducing the cracking risk of the tunnel lining, with an appropriate removal time of 48 h. This work provides insights into the thermal–mechanical behavior of lining concrete, thereby mitigating its early cracking in a high-geothermal environment.

Keywords: high-geothermal; lining concrete; thermal–mechanical coupling model; surrounding rock temperature; thermal insulation layer; curing condition

Academic Editor: Humberto Varum

Received: 13 December 2024
Revised: 14 January 2025
Accepted: 18 January 2025
Published: 20 January 2025

Citation: Xie, S.; Zhao, D.; Yi, P.; Chen, Q.; Liu, W. Investigation into the Early Cracking Behavior of High-Geothermal Tunnel Lining Concrete Based on Thermal–Mechanical Coupling Model. *Buildings* **2025**, *15*, 301. https://doi.org/10.3390/buildings15020301

1. Introduction

The tunnel, as an integral infrastructure in the transportation network, has emerged as a pivotal role in facilitating connectivity across inaccessible terrains, thereby improving transport efficiency [1–3]. Driven by the demand for transportation, the construction of deep-buried and extra-long tunnels has been growing in recent years, particularly in the mountainous regions of western China. However, a series of harsh geological conditions have been encountered during construction, with high-geothermal conditions standing out as a major engineering challenge [4,5]. For example, the maximum temperature of the surrounding rock reaches a magnitude of 88.8 °C, with an average level of above 70.0 °C in the Nige Tunnel in China [6]. Such thermal conditions usually accelerate the degradation of construction equipment, resulting in the need for additional cooling systems and an

increase in overall construction costs [7]. In addition, high-geothermal environments pose significant risks to the health and safety of workers, reducing productivity and increasing the potential for work-related accidents, as illustrated in [8].

To ensure the safety of high-geothermal tunnel construction, thermal insulation and ventilation measures have been extensively studied by numerical simulation [4,7,9]. Generally, applying a thermal insulation layer along the tunnel is an effective approach to reducing the intense heat dissipation from the surrounding rock, particularly when its temperature exceeds 50 °C [10]. Meanwhile, the thermal insulation effect is closely associated with the thickness and thermal conductivity of the layer [11]. In terms of ventilation, increasing speed and frequency is conducive to obtaining a superior cooling effect [12]. To keep the ambient temperature below 28 °C during tunnel construction, as suggested by [4], it is necessary to ventilate at a velocity greater than 3.5 m/s 3 times a day in the Gaoligongshan Tunnel. In addition, spraying and ice block cooling measures are usually adopted in high-geothermal tunnels, thereby providing a more comfortable construction environment for workers [7,13].

Indeed, high-geothermal conditions introduce a one-dimensional heat conduction field into the tunnel structure, significantly influencing the early properties of lining concrete [14]. According to [15,16], high temperature accelerates the hydration of cementitious materials within the concrete, reducing total porosity and improving the mechanical properties during the early stage. Despite this, rapid hydration induces an uneven distribution of hydrates, resulting in the formation of localized weak zones and a reduction in overall strength at 28 d, relative to the standard curing condition [17]. Furthermore, considering the dual effect of external geothermal source and internal hydration heat, significant thermal stress is generated within the concrete, leading to the formation of cracks [14,18]. Once cracks develop on the surface, aggressive agents in the environment are likely to penetrate into the concrete through the crack channels, compromising the load-bearing capacity and durability of tunnel structure [19]. As reported by [1], cracks are the most common defects in the highway tunnels of China, thereby leading to the necessity of investigating early cracking behavior in lining concrete.

Generally, the addition of supplementary cementitious materials (SCMs), such as fly ash and blast furnace slag, is conducive to mitigating cracking behavior by reducing the hydration heat and autogenous shrinkage of concrete [20]. Li et al. [21] further introduced a temperature rise inhibition and expansion agent, providing a feasible solution to prevent early cracking of the lining through dual regulation techniques in terms of temperature and deformation. In addition to mixture design, steam curing is an effective approach for reducing the temperature gradient and the cracking risk of lining concrete after casting, as illustrated in [18]. When evaluating the early cracking characteristics of concrete, several laboratory methods, including slab and ring tests, are usually employed to measure the amount, width and area of cracks [22]. Nevertheless, such results are inadequate to reveal directly the cracking mechanism in terms of structural level. Consequently, Liu et al. [23] illustrated the interaction between concrete and the environmental factors, such as temperature, humidity and constraint, during the early stage, and further proposed a reliability-based strategy to assess the cracking risk of hardening concrete. Based on the coupled thermal–mechanical model, Peng et al. [24] believed that the cracking behavior of concrete in a high-temperature environment first occurs at the interfacial transition zone (ITZ) and gradually evolves into more penetrating cracks. Moreover, Wang et al. [25] conducted field experiments and observed that high temperature induces significant tensile stresses on the external surface of the lining vault, raising the cracking risk in the tunnel lining. Despite these previous studies, the property evolution of concrete, such as hydration heat and tensile strength, closely related to cracking behavior, is usually neglected in

thermal–mechanical analysis. In addition, parameter studies on the cracking risk of tunnel lining, considering construction conditions, remain relatively limited.

Based on a high-geothermal environment, this work aims to explore the early cracking behavior of tunnel lining through thermal–mechanical coupling simulation. Firstly, the early property evolution of concrete was determined by laboratory experiments and empirical functions. A finite element model was then established to analyze the temperature and stress fields of tunnel lining, and its reliability was further validated by field experiments. Finally, several factors, such as surrounding rock temperature, thermal insulation, and curing conditions, were analyzed by adjusting the model. This work provides theoretical support for tunnel construction in a high-geothermal environment, thereby reducing the early cracking risk for lining concrete.

2. Background and Theory

2.1. Topography

The tunnel in this study is a double-track railway tunnel in western China, with a total length of 20.79 km and a maximum buried depth of 1219 m. The tunnel site is on the edge of the Tibet Plateau with an altitude ranging from 3500 to 4700 m, and the surrounding rocks are characterized by biotite monzonitic granite. The tunnel passes through the Yunongxi active fault with its adverse geological conditions, such as high-geothermal activity and rock explosion, making it a typical first-class risk tunnel. Considering the diffusion of geothermal flux from the cracks in the surrounding rock [4,25], high-geothermal conditions were significant during the tunnel construction, with a maximum temperature of 82.1 °C measured by detecting holes. Notably, the quality inspection reveals over 20 cracks on the external surface of the lining in the high-geothermal zone, from DK281+520 to DK282+580, after removing the formwork at 2 d.

2.2. Materials

In the tunnel support system, shotcrete of grade C25 and cast-in-situ concrete of C35 were utilized for the initial support and secondary lining, respectively. Their thermal and mechanical property parameters are listed in Table 1. To obtain the early property evolution of lining concrete, laboratory experiments, including studies of hydration heat and mechanical properties, were conducted, according to the mixture proportion in Table 2.

Table 1. Property parameters of concrete.

Materials	Elastic Modulus (GPa)	Compressive Strength (MPa)	Poisson's Ratio	Thermal Expansion Coefficient (1/°C)	Thermal Conductivity ($W \cdot (m \cdot K)^{-1}$)	Specific Heat ($J \cdot (kg \cdot °C)^{-1}$)
Shotcrete	23.2	31.5	0.25	7.8×10^{-6}	920	3.0
Lining concrete	24.9	43.1	0.20	8×10^{-6}	840	1.9

Table 2. Mixture proportion for lining concrete (kg/ m^3).

Water	Cement	Fly Ash	Fine Aggregate	Coarse Aggregate
166	260	110	784	1000

For raw materials, ordinary Portland cement (OPC) of type P.II.42.5(R) was manufactured by Taini Cement Co., Ltd., (Jurog City, China) following Chinese Standard GB175-2023 [26]. Fly ash was supplied by Sichuan Luzhou Power Plant, with a loss on ignition of 3.5% and an activity index of 91%. Fine aggregate was derived from the medium-grade river sand in Chengdu, whereas coarse aggregate with a particle size range of 5–25 mm was

collected from local crushed stone. During the experiment, the heat evolution of cementitious materials was monitored by an isothermal calorimeter (TAM Air, TA Instruments, New Castle, DE, USA), as depicted in Figure 1a. According to Chinese Standard GB/T 50081-2019 [27], the mechanical properties of concrete, measured by a compressive testing instrument (TYE-1000 E, Wuxi Jianyi Instrument Equipment Co., Ltd., Wuxi, China), are presented in Figure 1b.

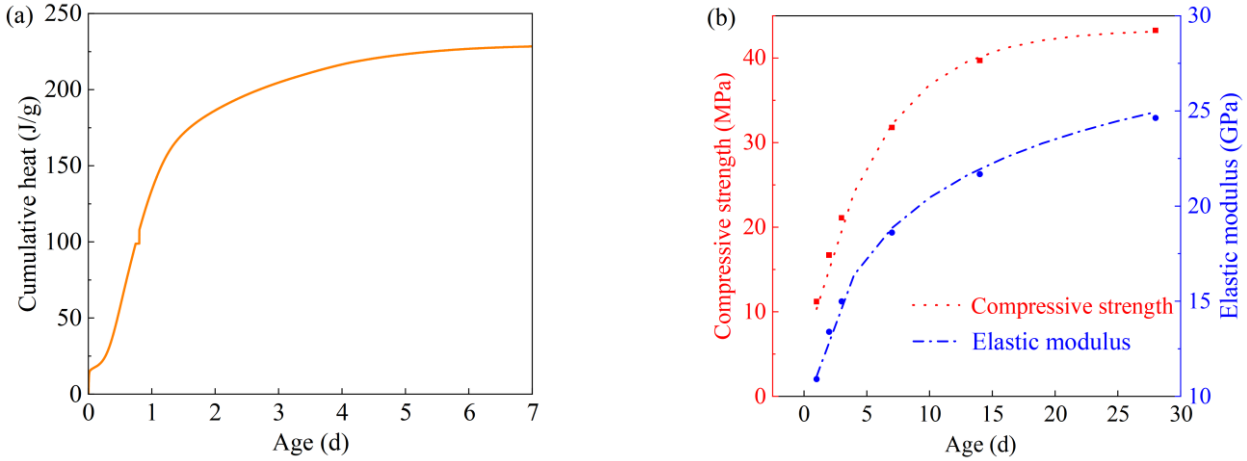

Figure 1. Early property evolution of lining concrete: (**a**) hydration heat and (**b**) mechanical properties.

Results indicate that the cumulative heat of the mixture increased as hydration progressed, with a significant increase from 0 to 2 d, as reported by [14]. Notably, the hydration degree reached 81.3% at 2 d, and tended to stabilize at 7 d. With the curing age, both the compressive strength and elastic modulus exhibited a growing trend, especially pronounced at 1–7 d.

2.3. Calculation Theory

2.3.1. Heat Transfer Mechanism

The heat transfer mechanism of the high-geothermal tunnel is described in Figure 2. Heat conduction, as the primary form of the whole process, occurs from the depth of the rock to the tunnel lining, thereby increasing the airflow temperature within the tunnel [28]. To mitigate this process, a thermal insulation layer is usually designed between the initial support and the secondary lining [29,30]. Meanwhile, the airflow within the tunnel is subject to heat convection, leading to a uniform distribution of the overall temperature [31]. In addition, it is necessary to consider hydration in the heat transfer mechanism during the early stage [12], as expressed in Equation (1):

$$\frac{\partial T}{\partial \tau} = \alpha\left(\frac{\partial^2 T}{\partial x^2} + \frac{\partial^2 T}{\partial y^2} + \frac{\partial^2 T}{\partial z^2}\right) + \frac{\partial \theta}{\partial \tau} \quad (1)$$

where T denotes the temperature of any microelement dxdydz in the concrete; τ represents the concrete age; θ is the adiabatic temperature rise due to cement hydration; and α is the thermal diffusivity of concrete.

To obtain the unique solution to Equation (1), it is necessary to determine the relevant initial and boundary conditions. Theoretically, the initial temperature is constant and uniformly distributed, and its value is the molding temperature of concrete [32,33]. In addition, the heat convection boundary is adopted, according to the heat transfer model, as shown in Equation (2):

$$-\lambda \frac{\partial T_a}{\partial n} = \beta(T_a - T_b) \quad (2)$$

where T_a and T_b denote the temperatures of concrete surface and environment, respectively; λ and β represent the heat conduction and convection coefficients, respectively; and n is the direction normal to the surface.

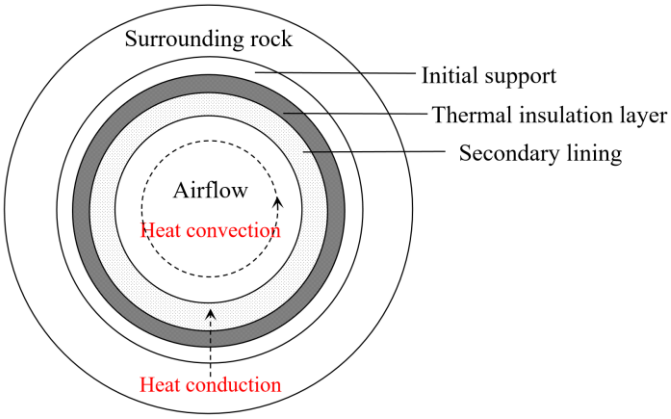

Figure 2. Heat transfer mechanism of high-geothermal tunnel.

2.3.2. Environmental Temperature

To obtain the heat convection boundary related to Equation (2), the ambient temperature of the tunnel was monitored by a data collector during the first 7 d after casting, as shown in Figure 3. Generally, a sinusoidal function is employed to fit the environmental temperature [25,34], as expressed in Equation (3):

$$T_b(\tau) = T_m + \frac{A_n}{2} \cdot \sin\left[\frac{\pi(\tau - a_1)}{b_1}\right] \quad (3)$$

where $T_b(\tau)$ is the environmental temperature at the age of τ; T_m is the average temperature; A_n represents the amplitude of temperature; and a_1 and b_1 denote the constants. The above parameters were determined by fitting the measured curves, i.e., $T_m = 23.8$ °C, $A_n = 6$ °C, $a_1 = -0.94$ and $b_1 = 0.50$.

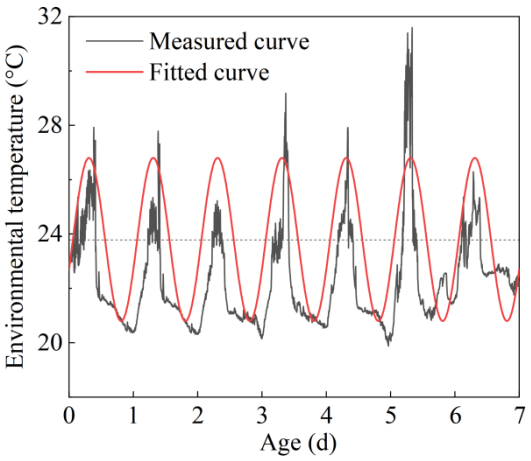

Figure 3. Measured and fitted curves for environmental temperature.

2.3.3. Adiabatic Temperature Rise of Concrete

Considering the ongoing hydration, adiabatic temperature rise is a key factor for the balance of Equation (1), calculated by the relevant hydration heat patterns of cementi-

tious materials within the concrete [23,35]. The common fitting formula is the composite exponential function, as shown in Equation (4):

$$Q(\tau) = Q_0\left(1 - e^{-a_2\tau^{b_2}}\right) \tag{4}$$

where $Q(\tau)$ is the cumulative hydration heat at the age of τ; Q_0 is the total cumulative hydration heat; and a_2 and b_2 represent the constants. Based on the evolution of hydration heat in Figure 1a, the corresponding parameters were obtained, i.e., $Q_0 = 2.28 \times 10^5$kJ/kg, $a_2 = 1.15$ and $b_2 = 0.76$. The adiabatic temperature rise is further calculated according to Equation (5):

$$\theta(\tau) = \frac{Q(\tau)(W + kF)}{c\rho} \tag{5}$$

where $\theta(\tau)$ is the cumulative adiabatic temperature rise; W and F are the amount of cement and fly ash, respectively; k represents the discount factor of mineral admixture, taking 0.25; and c and ρ denote the specific heat capacity and density of concrete, respectively.

2.3.4. Mechanical Properties of Concrete

The mechanical properties of concrete exhibit dynamic evolution during the early curing stage, closely related to its stress field [36,37]. Generally, the compressive strength of concrete is expressed as an exponential function, as shown in Equation (6):

$$f_{cu,\tau} = a_3 + b_3 e^{-c_3\tau} \tag{6}$$

where $f_{cu,\tau}$ is the compressive strength at the age of τ; and a_3, b_3 and c_3 represent the constants. The above parameters were determined by analyzing the patterns in Figure 1b, i.e., $a_3 = 43.40$, $b_3 = -39.60$ and $c_3 = 0.18$. The tensile strength $f_t(\tau)$, as an indicator of the cracking resistance of concrete, is further calculated by Equation (7):

$$f_t(\tau) = 0.332 {f_{cu,\tau}}^{0.60} \tag{7}$$

Furthermore, a double exponential function is adopted to evaluate the elastic modulus of concrete at its early age, as shown in Equation (8):

$$E(\tau) = E_0\left(1 - e^{-a_4\tau^{b_4}}\right) \tag{8}$$

where $E(\tau)$ is the elastic modulus at the age of τ; E_0 is the ultimate elastic modulus; and a_4 and b_4 denote the constants. The mentioned parameters were calculated based on Figure 1b, i.e., $E = 32.2$ GPa, $a_4 = 0.42$ and $b_4 = 0.38$.

2.3.5. Thermal–Mechanical Coupling Procedures

According to the thermal–mechanical coupling method, the heat transfer model was developed to obtain the temperature field, and then the stress field was further analyzed based on the temperature loading [24,25,38], as shown in Figure 4. The elements of DC3D8R and C3D8R were employed in the thermal and mechanical analysis, respectively. In addition, the time-dependence of environmental temperature, adiabatic temperature rise and mechanical properties, as described in Sections 2.3.2–2.3.4, were inserted into the finite element model by Fortran subroutines, including FILM, HETVAL and USDLD, respectively. Notably, the thermal analysis was unsteady considering the adiabatic temperature rise of concrete, and the mechanical analysis was nonlinear considering the increase in elastic modulus of the early-age concrete.

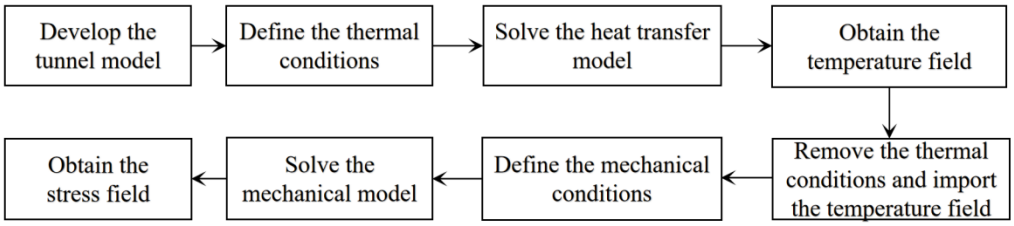

Figure 4. Thermal–mechanical coupling procedures.

3. Numerical Model

3.1. Model Establishment

The overall model, shown in Figure 5a, was developed by ABAQUS software with a plane dimension of 100 m × 100 m and a longitudinal thickness of 12 m. The standard tunnel cross-section was in the shape of a horseshoe, with a width of 16.44 m and a height of 12.29 m. The composite lining was utilized for tunnel support, comprising an initial support with a thickness of 0.23 m and a secondary lining with a thickness of 0.40 m, as described in Figure 5b.

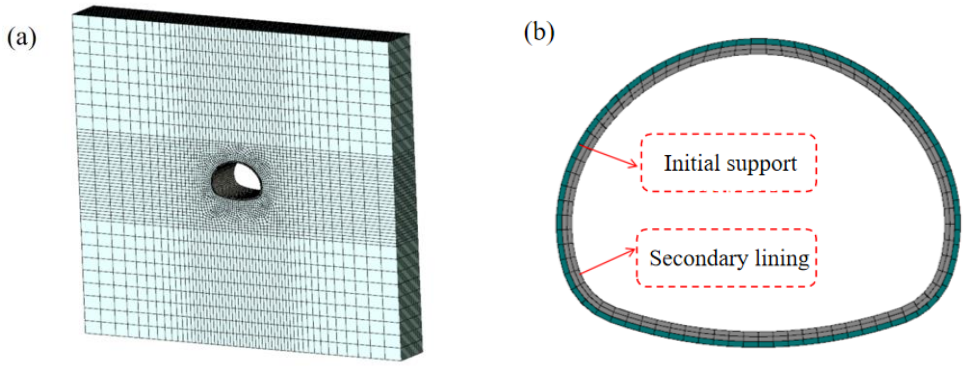

Figure 5. Finite element model: (**a**) overall model and (**b**) tunnel cross-section.

The initial temperatures of surrounding rock and tunnel environment were set at 50 °C and 23 °C, respectively. The construction process was conducted by one-time full-section casting, and the formwork was removed at the curing age of 48 h. For the boundary of the temperature field, the heat convection coefficient of the lining external surface was set at 20 W/(m^2·°C) under a fully ventilated condition, while its value is only 50% before the formwork removal [39,40]. For the boundary of the stress field, the surrounding rock was subjected to a series of deformation restrictions, and uniformly distributed surface loads in the horizontal and vertical direction were applied to simulate the surrounding rock pressures, according to Chinese Standard TB10003-2016 [41].

3.2. Model Analysis

3.2.1. Temperature Field

The temperature field of the lining during the initial 7 d after casting was analyzed, with 1 h and 7 d depicted in Figure 6a,b. Meanwhile, the characteristic nodes, including Node-A and Node-B, in the middle of sidewall were extracted, as shown in Figure 6c. Node-A was the internal node in direct contact with the initial support, and Node-B was the external node connected to the tunnel environment. Their time–history patterns of temperature are described in Figure 6d.

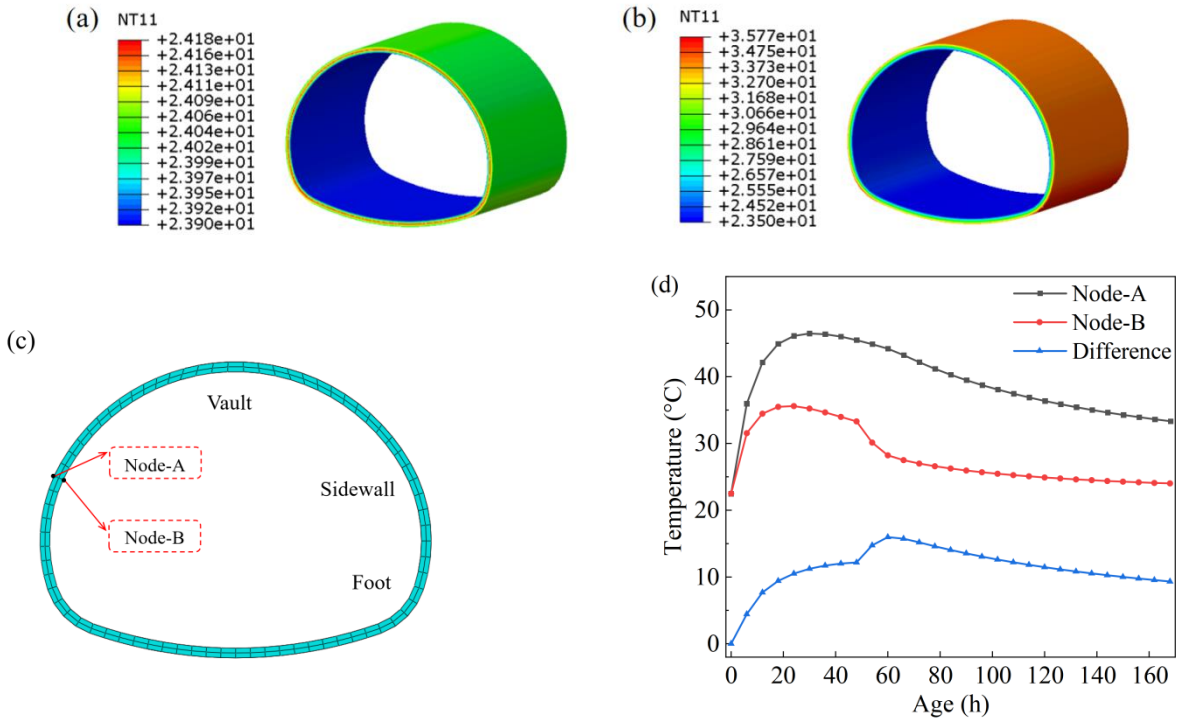

Figure 6. Temperature field analysis: temperature contour maps at (**a**) 1 h, (**b**) 7 d (unit: °C); and (**c**) location and (**d**) time–history curves of the temperature characteristic nodes.

At the early age of 1 h, the internal and external surface temperatures of the lining increased to approximately 24 °C due to hydration, despite no significant difference. After 1 d of casting, both the internal and external surfaces of the lining reached the highest temperature. Notably, the peak temperature of the former was greater than that of the latter, due to the stronger effect of high-geothermal conditions on the internal surface, as reported by [14]. After removing the formwork at 2 d, the heat convection between the lining concrete and the external environment was enhanced, leading to a significant decrease in the temperature of the lining external surface [39]. When the age reached 7 d, the temperatures of the internal and external surfaces were 35.78 °C and 23.50 °C, respectively, indicating a greater temperature gradient within the concrete. Considering the lower adiabatic temperature rise caused by hydration at 7 d [16,35], the temperature field was mainly influenced by the high-geothermal conditions at this moment. Furthermore, it is observed that the temperature difference between the internal and external surfaces exhibited an increasing and then decreasing trend, with the maximum temperature difference occurring at 60 h and reaching 15.98 °C.

3.2.2. Stress Field

The mechanical model of lining concrete was further solved to obtain the stress fields at 1 h and 7 d, as shown in Figure 7a,b. After 1 h of casting, tensile stress occurred in certain zones of the lining external surface, and the maximum tensile stress was concentrated in the sidewall. When the age reached 7 d, tensile stresses were distributed on the whole external surface of sidewall, with a highest level of 1.06 MPa.

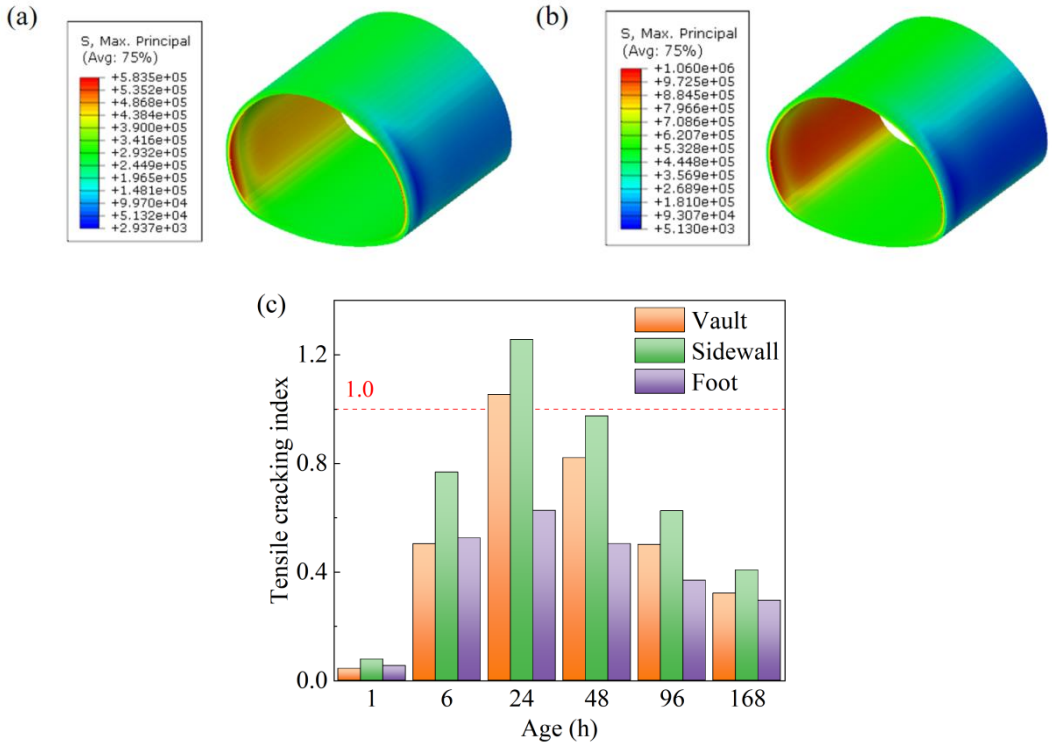

Figure 7. Stress field analysis: stress contour maps at (**a**) 1 h, (**b**) 7 d (unit: Pa); and (**c**) tensile crack indices for different zones and curing ages.

To study the correlation between the cracking behavior of concrete and stress distribution, tensile cracking index η is introduced [23,42], as expressed in Equation (9):

$$\eta = \frac{\sigma_\tau}{f_t(\tau)} \tag{9}$$

where σ_τ and $f_t(\tau)$ denote the maximum tensile stress and tensile strength of concrete at the age of τ, respectively, where the tensile strength is calculated based on Equation (7). When $\eta > 1$, cracks develop within the concrete due to the tensile action. The tensile cracking indices for different zones of the lining (i.e., vault, sidewall and foot) at different ages are presented in Figure 7c.

At the age of 24 h, the tensile cracking indices of the vault and sidewall were 1.05 and 1.26, respectively, indicating a higher cracking risk in the lining sidewall. On the one hand, the lining is subjected to the dual effect of external geothermal flux and the internal heat source from hydration during the early stage, significantly increasing the overall temperature of concrete [14]. On the other hand, the temperature of the external surface decreases, due to the heat exchange with the tunnel environment [10,40]. Both of these effects lead to a steep temperature gradient within the concrete, thereby generating thermal stress [18]. Moreover, the lining endures the effects of the stress field induced by the external load from the surrounding rock. These thermal and mechanical stresses introduce a condition that is highly conducive to the formation of cracks when the tensile strength of concrete is inadequate to withstand such stress levels, particularly during the initial days after casting, as illustrated in [19,24]. As the curing age prolonged, the mechanical properties were further enhanced, leading to a decrease in the tensile cracking index. For example, when the age reached 4 d, the tensile cracking indices for different zones of the lining were less than 0.70, indicating a lower cracking risk in the overall tunnel lining.

3.3. Model Validation

To validate the reliability of the model, the tunnel lining temperature was monitored for the initial 7 d after casting, as shown in Figure 8a–c. In more detail, three equal-distance monitoring nodes (I-III) were first determined on the lining sidewall in the longitudinal direction. Afterwards, PT100 thermal couples, with an accuracy of 0.5 °C in the range of −30 to 100 °C, were installed on the surface of the initial support and the outermost side of the lining reinforcement mesh for each monitoring node, corresponding to the internal and external surface of the lining, respectively [25]. After casting the lining concrete, data collectors of type LR8401-21, powered by a mobile battery with a capacity of 98,000 mAh, were employed to measure the temperature evolution. The results are given in Figure 8d.

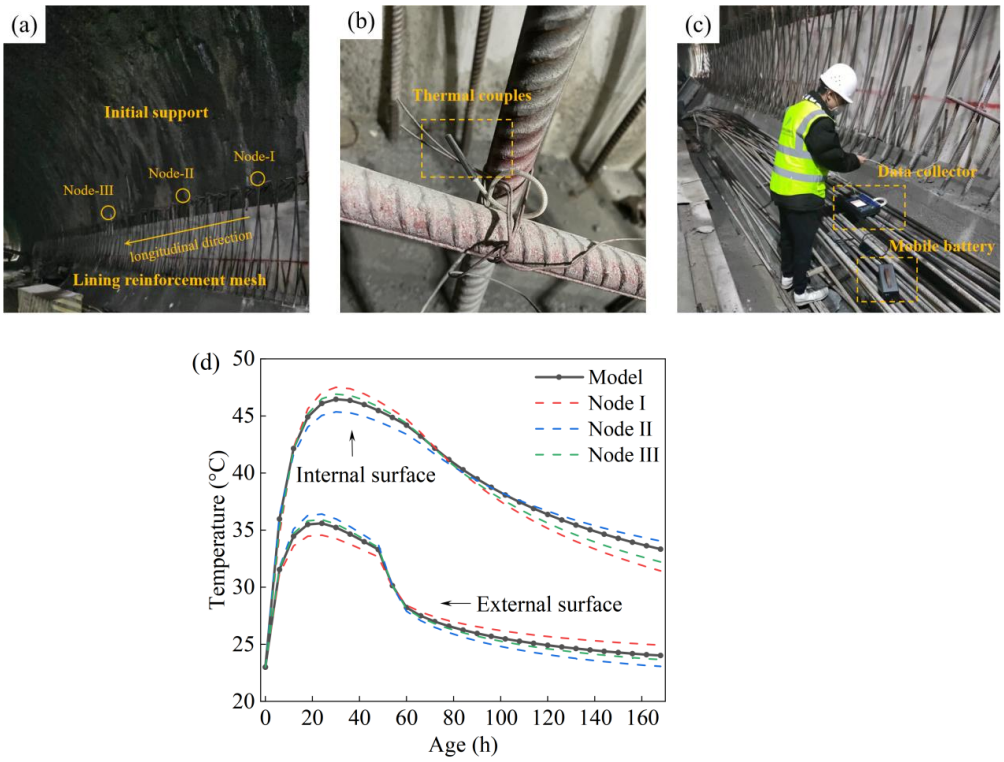

Figure 8. Model validation: (**a**) determining the monitoring nodes, (**b**) installing the thermal couplings, (**c**) monitoring on-site and (**d**) validating the results.

Trends indicate that the temperature evolution measured by monitoring nodes I–III were roughly consistent with those calculated by the model. Notably, the maximum absolute percentage errors in the internal and external surface temperatures of lining concrete were 6.07% and 3.98%, respectively. These deviations are attributed to the complicated heat transfer patterns, including high-geothermal, hydration heat and external ventilation conditions in the tunnel, as well as the uncertainty stemming from on-site construction. In conclusion, the above model is reasonable, effectively reflecting the early temperature evolution of tunnel lining.

4. Parameter Analysis

4.1. Surrounding Rock Temperature

As the thermal boundary condition of the model, surrounding rock temperature plays an important role in the temperature and stress fields of the tunnel lining during the early stage [43,44]. According to the possible surrounding rock temperature encountered during construction, five conditions, ranging from 50 to 90 °C with an increment of 10 °C, are analyzed according to the model in Section 3.1. The temperature evolution curves of Node-A

and Node-B, and their maximum temperature differences under different conditions, are shown in Figure 9a,b, respectively.

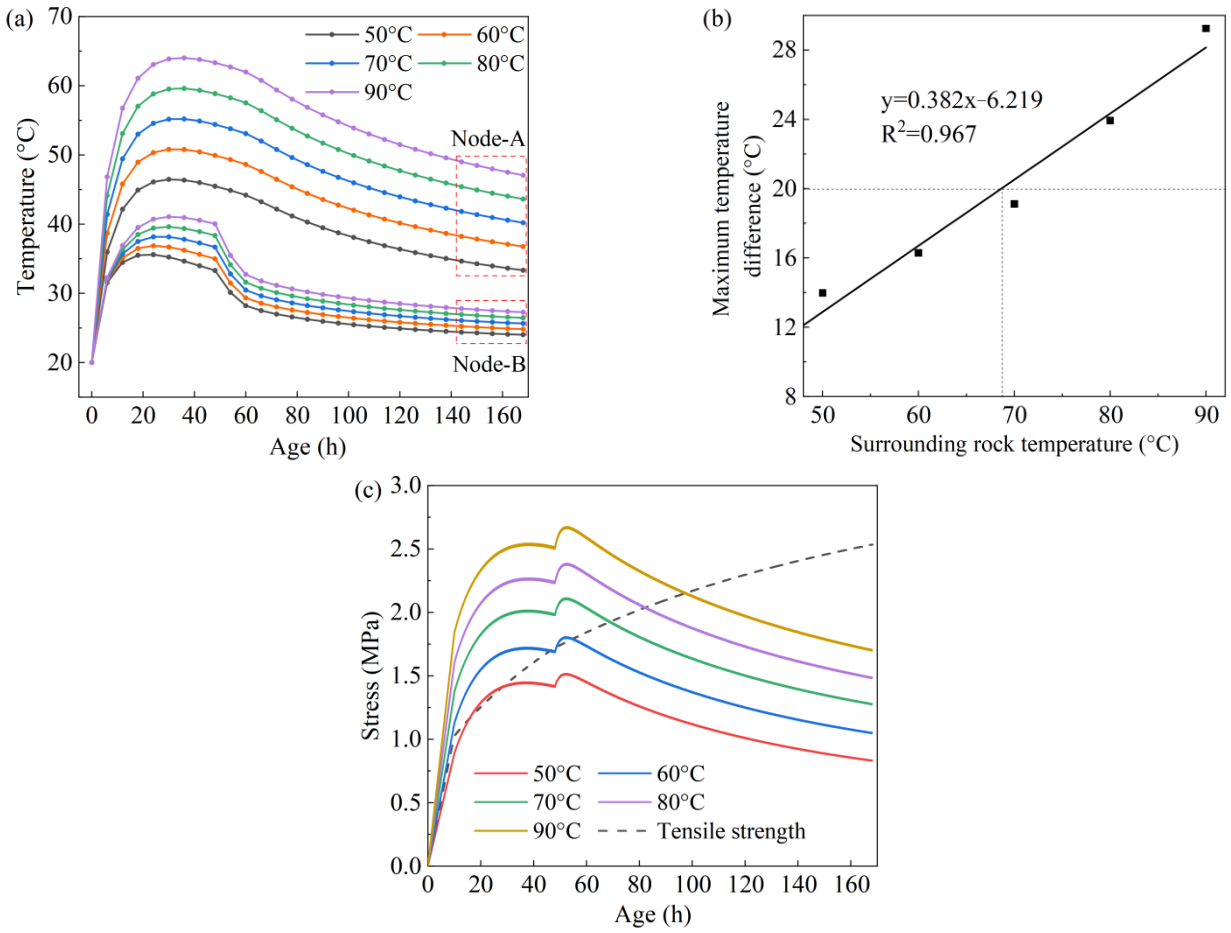

Figure 9. Effect of surrounding rock temperature on cracking behavior of lining concrete: (**a**) temperature evolution; (**b**) maximum temperature difference; and (**c**) stress evolution.

The evolution trends for Node-A and Node-B exhibited no significant differences under various conditions, with peak temperatures at around 24 h. Meanwhile, it is observed that their maximum temperature differences were linearly related to the surrounding rock temperature. Following Chinese Standard Q-CR 9604-2015 [45], it is advisable that the temperature difference between the internal and external surfaces is below 20 °C after removing the formwork, which provides a controlled indicator for evaluating the cracking risk of lining concrete. When this indicator is 20 °C, the surrounding rock temperature is determined as 68.7 °C, according to Figure 9b. Consequently, at a surrounding rock temperature above 68.7 °C, the cracking risk of lining is considered to be high, leading to the need for thermal insulation measures, similar to those in [10].

Figure 9c presents the time–history curves of Node-B (related to the external surface of rgw lining sidewall) under various conditions. With the curing age, the stress level of Node-B exhibited an overall increasing and then decreasing trend, reaching peak stress at around 52 h. Notably, removing the formwork accelerated the heat convection between concrete and the external environment [39], resulting in a significant increase in tensile stress at 48 h. Specifically, for a surrounding rock temperature of 60 °C, the time–history peak tensile stress was 1.81 MPa, and the stress level was higher than the tensile strength at the same age for 0–52 h after casting, up to 23.6%. When the surrounding rock temperature reached 90 °C, the time–history tensile stress peaked at 2.67 MPa, exceeding the tensile strength of the

same age by 51.0%, and tensile crack indices were above 1 at the age of 0–90 h. The above findings indicate that tensile stress levels and cracking risk duration of the lining increases with the surrounding rock temperature, aligning with the patterns in [25].

4.2. Thermal Insulation Layer

Thermal insulation materials are usually laid in the tunnel construction in a high-geothermal environment, including silicate composite and rigid polyurethane [9,46], as listed in Table 3. The models were established to compare their thermal insulation effects, where thermal insulation layer was designed as a sandwiched structure with a thickness of 20 mm and the surrounding rock temperature was 90 °C. Finally, the temperature contour maps were obtained, as described in Figure 10. It is observed that, when adopting silicate composite materials, the temperatures on both sides of thermal insulation layer were 76 °C and 43 °C, respectively. For rigid polyurethane materials, the corresponding values were 80 °C and 39 °C, indicating its superior thermal insulation effect due to lower thermal conductivity, consistent with the observations in [10].

Table 3. Property parameters of thermal insulation materials.

Materials	Density (kg/m^3)	Thermal Expansion Coefficient (1/°C)	Thermal Conductivity (W·(m·K)$^{-1}$)	Specific Heat (J·(kg·°C)$^{-1}$)
Silicate composite	80	5.0×10^{-6}	0.045	1100
Rigid polyurethane	30	7.8×10^{-6}	0.027	920

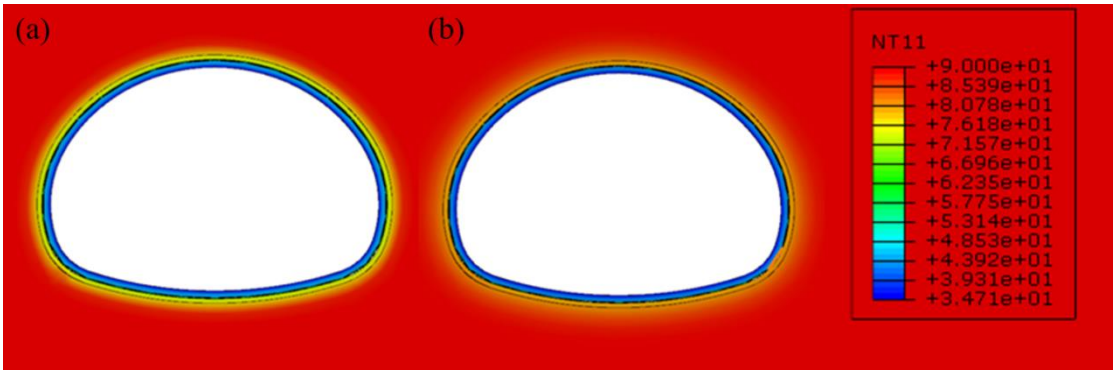

Figure 10. Temperature contour maps for laying different insulation materials: (**a**) silicate composite and (**b**) rigid polyurethane (unit: °C).

The models were further adjusted considering the position of the thermal insulation layer, i.e., sandwiched and wall-attached structures [12]. The time–history curves of temperature difference between the internal and external surfaces under different laying positions, are shown in Figure 11a. Results indicate that the maximum temperature difference was 29.3 °C without thermal insulation. When laying in a sandwiched structure, the corresponding value was 12.5 °C, indicating the inhibited heat conduction process from the surrounding rock to the tunnel lining. In addition, adopting wall-attached structures was conducive to reducing the heat convection between the lining concrete and the external environment, achieving a maximum temperature difference of up to 16.0 °C. However, in this case, the lining structure was exposed to high temperature for a long term, thereby reducing the durability of the tunnel lining [47]. Therefore, a sandwiched structure is more suitable for thermal insulation in the high-geothermal tunnel.

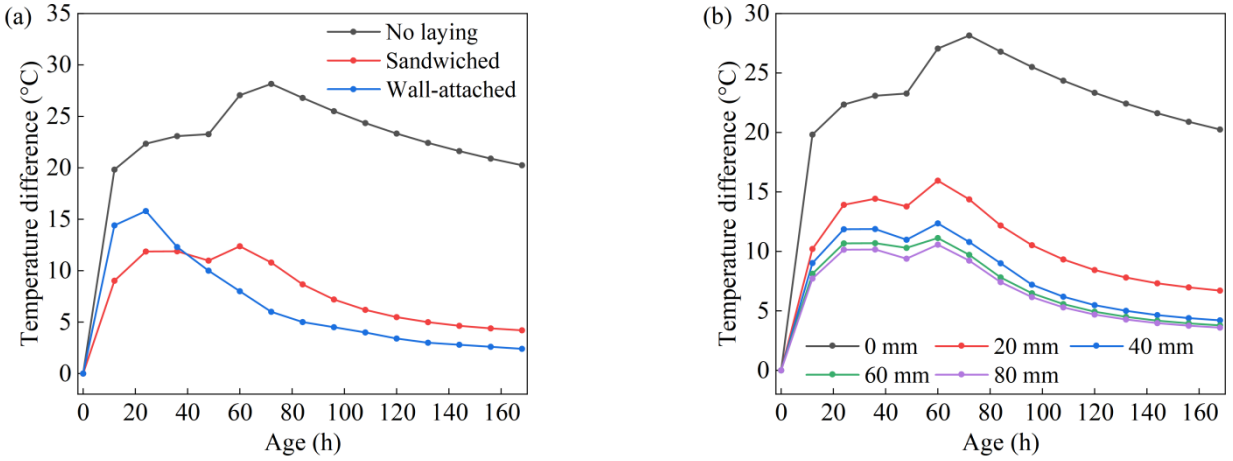

Figure 11. Effect of (**a**) position and (**b**) thickness of thermal insulation layer on temperature evolution of lining concrete.

In addition to the material properties and laying positions, thickness is a critical parameter for the thermal insulation layer [11]. The effect of the thickness of the thermal insulation layer on the maximum temperature difference is presented in Figure 11b. It is observed that, as the thickness increased from 20 to 40 mm, the maximum temperature difference decreased by 43.6% and 56.0%, respectively, compared to the condition without thermal insulation. However, the condition with a thickness of 80 mm exhibited no significant differences from that with a thickness of 60 mm, indicating a plateau at a certain thickness, similar to the observations in [43]. Notably, an increase in layer thickness is generally associated with higher construction costs, resulting in the necessity to control the thickness of the thermal insulation layer within 60 mm. Combined with Chinese Standard Q-CR 9604-2015 [45], a thickness range of 20–60 mm is conducive to achieving a superior thermal insulation effect at a low cost.

4.3. Curing Condition

4.3.1. Formwork Heat Convection Properties

During the early curing stage, formwork plays a key role in heat exchange with the external environment [39,48]. Based on the model in Section 3.1, the temperature and stress evolution of the lining was studied when applying formwork with different heat convection coefficients, as depicted in Figure 12.

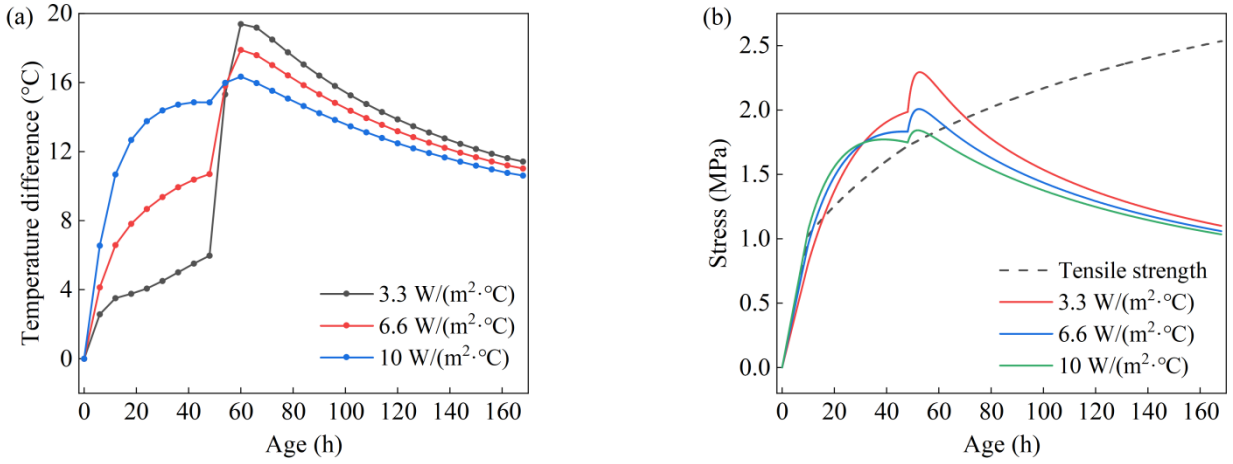

Figure 12. Effect of formwork heat convection coefficient on cracking behavior of lining: (**a**) temperature and (**b**) stress evolution.

Considering the formwork removal at 48 h, the temperature difference between the internal and external surfaces exhibited a significant increase, particularly under the condition with heat convection coefficients of 3.3 W/(m^2·°C), up to 9.34 °C. In this case, the heat sourced from the high-geothermal conditions and hydration accumulated within the lining concrete, generating a lower temperature gradient before removing the formwork [14]. However, the lining concrete underwent intense heat convection with the external environment due to the formwork unloading, resulting in a drop in the external surface temperature and a significant increase in the temperature gradient of concrete [44]. In addition, the time–history peak tensile stress at a heat convection coefficient of 10 W/ (m^2·°C), was higher than that at a heat convection coefficient of 3.3 W/(m^2·°C), indicating superior curing conditions and lower cracking risk of lining concrete when adopting formwork with a larger heat convection coefficient.

4.3.2. Formwork Removal Time

Removal time of formwork is an important factor in the construction progress and in the early cracking behavior of tunnel lining [32]. The temperature and stress evolution of concrete for various formwork removal times was further analyzed by adjusting the model parameters, as depicted in Figure 13.

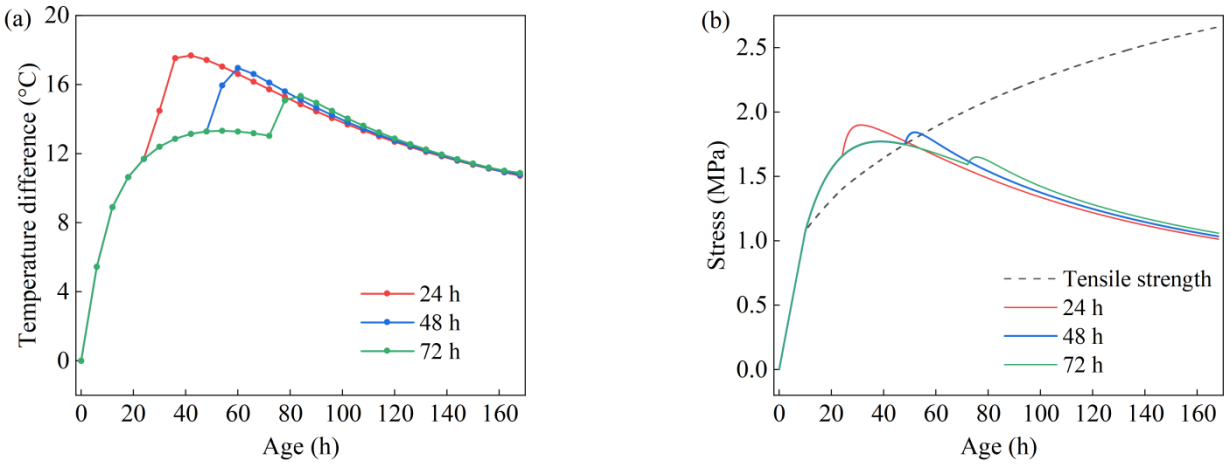

Figure 13. Effect of formwork removal time on cracking behavior of lining: (**a**) temperature and (**b**) stress evolution.

As the formwork removal time prolonged, the maximum temperature differences for various conditions were 17.69, 16.96 and 15.34 °C, corresponding to the ages of 42, 60 and 84 h, respectively. This indicates that the increase in formwork removal time is conducive to decreasing the concrete temperature gradient and delaying the onset of maximum temperature difference, thereby reducing the cracking risk of lining, as reported by [25,33]. Furthermore, when the formwork was removed at 24 h, the time–history tensile stress reached a peak of 1.94 MPa at approximately 30 h, exceeding 32.9% of the tensile strength at the same age. In comparison, for the formwork removal at 72 h, the time–history tensile stress peaked at 1.65 MPa after 75 h of casting, which was 15.3% lower than the corresponding tensile strength. Notably, lining concrete exhibited higher tensile strength when removing the formwork at 48 h, roughly meeting the requirement of early cracking resistance. Although delaying the formwork removal from 48 to 72 h is conducive to further reducing the time–history tensile stress, it has an adverse effect on the construction progress. Consequently, it is more suitable to remove the formwork at 48 h.

5. Conclusions

In this study, the early cracking behavior of tunnel lining exposed to high-geothermal environment is analyzed based on the thermal–mechanical coupling model. The primary conclusions are briefly summarized as follows.

(1) Considering the effect of geothermal source, the temperature of the internal surface is higher than that of the external surface, with the temperature difference reaching a peak of 15.98 °C at 60 h. In terms of stress field, the higher cracking risk occurs on the external surface of the lining sidewall at 24 h, and the cracking risk for the tunnel lining gradually decreases after 24 h.

(2) The maximum temperature difference within the lining structure is linearly related to the surrounding rock temperature. When the surrounding rock temperature exceeds 68.7 °C, thermal insulation measures for the tunnel lining are necessary. In addition, the tensile stress levels and cracking risk duration of the lining structure greatly increase with the surrounding rock temperature.

(3) For thermal insulation, laying a sandwiched structure with rigid polyurethane materials not only reduces the heat conduction from geothermal source to tunnel structure, but also ensures the durability of the lining concrete. A layer thickness range of 20–60 mm is conducive to achieving superior thermal insulation at a low cost.

(4) During the curing stage, applying formwork with a larger heat convection coefficient is an effective approach to decrease the temperature gradient caused by the formwork removal, mitigating the cracking behavior of the tunnel lining. Considering the construction progress, it is more appropriate to remove the formwork at 48 h.

In summary, this study provides theoretical approaches to reduction of the cracking risk of lining concrete in the high-geothermal conditions. In future work, it will be possible to further optimize the coupled model by considering creep behavior and moisture transport within the concrete, along with an exploration of the cracking behavior of tunnel lining in other extreme environments.

Author Contributions: Data curation, writing—original draft, S.X.; formal analysis, investigation, D.Z.; methodology, visualization, conceptualization, P.Y.; writing—review and editing, investigation, Q.C.; conceptualization, funding acquisition, supervision, writing—review and editing, W.L. All authors have read and agreed to the published version of the manuscript.

Funding: This work was funded by the National Natural Science Foundation of China (51978408, 51978414, 51678368) and the Guangdong Provincial Key Laboratory of Durability for Marine Civil Engineering (SZU) (2020B1212060074).

Data Availability Statement: The original contributions presented in the study are included in the article, further inquiries can be directed to the corresponding author.

Acknowledgments: We sincerely express our gratitude to the peer reviewers and editors for their professional comments for improving the manuscript.

Conflicts of Interest: Author Si Xie was employed by the company China Railway First Survey and Design Institute Group Co., Ltd. Author Dan Zhao was employed by the company Shenzhen Municipal Design and Research Institute Co., Ltd. The remaining authors declare that the research was conducted in the absence of any commercial or financial relationships that could be construed as a potential conflict of interest.

References

1. Ye, F.; Qin, N.; Liang, X.; Ouyang, A.H.; Qin, Z.; Su, E.J. Analyses of the defects in highway tunnels in China. *Tunn. Undergr. Space Technol.* **2021**, *107*, 103658. [CrossRef]

2. Lu, C.F.; Cai, C.X. Challenges and countermeasures for construction safety during the Sichuan-Tibet railway project. *Engineering* **2019**, *5*, 833–838. [CrossRef]
3. Zhu, H.H.; Yan, J.X.; Liang, W.H. Challenges and development prospects of ultra-long and ultra-deep mountain tunnels. *Engineering* **2019**, *5*, 384–392. [CrossRef]
4. Zeng, Y.H.; Tao, L.L.; Ye, X.Q.; Zhou, X.H.; Fang, Y.; Fan, L.; Liu, X.R.; Yang, Z.X. Temperature reduction for extra-long railway tunnel with high geotemperature by longitudinal ventilation. *Tunn. Undergr. Space Technol.* **2020**, *99*, 103381. [CrossRef]
5. Kong, F.M.; Xue, Y.G.; Gong, H.M.; Jiang, X.D.; Song, Q.; Fu, Y.S.; Fu, K. The formation mechanism of dynamic water and mud inrush geohazard triggered by deep-buried tunnel crossing active fault: Insights from the geomechanical model test. *Tunn. Undergr. Space Technol.* **2023**, *142*, 105437. [CrossRef]
6. Zhou, P.; Feng, Y.; Zhou, F.C.; Wei, Z.Q.; Gou, S.J.; Xu, H.B.; Wang, Z.J. Evaluation system of worker comfort for high geothermal tunnel during construction: A case study on the highway tunnel with the highest temperature in China. *Tunn. Undergr. Space Technol.* **2023**, *135*, 105028. [CrossRef]
7. Zhao, K.M.; Ji, W.H.; Cao, X.L.; Yuan, Y.P.; Li, H.C. Evaluation of cooling measures performance and thermal-humidity environment for ultra-high geothermal railway tunnel construction by using WBGT. *Eng. Appl. Comput. Fluid Mech.* **2024**, *18*, 2357725. [CrossRef]
8. Hu, Y.P.; Wang, M.N.; Wang, Q.L.; Liu, D.G.; Tong, J.J. Field test of thermal environment and thermal adaptation of workers in high geothermal tunnel. *Build. Environ.* **2019**, *160*, 106174.
9. Xu, Y.; Li, Z.J.; Wang, J.J.; Lu, Y.B.; Cheng, Z.; Wang, J.K.; Lin, Z. Improving thermal environment and ventilation efficiency in high-temperature excavation tunnels via an innovative heat insulation and cooling baffle. *Therm. Sci. Eng. Prog.* **2024**, *55*, 102992. [CrossRef]
10. Wang, Y.; Zhou, X.H.; Liu, X.R.; Qi, Z.F.; Li, N.; Chen, X. Cooling effect and parameter analysis of applying heat insulation layer to tunnel regionalization in construction period based on geothermal level. *Int. J. Therm. Sci.* **2025**, *208*, 109413. [CrossRef]
11. Qin, Y.P.; Hou, H.A.; Guo, M.Y.; Liu, Q.; Tang, F. Simulated and experimental study on effect of thermal insulation layer on temperature field and heat dissipation of roadway surrounding rock. *Case Stud. Therm. Eng.* **2024**, *53*, 103960. [CrossRef]
12. Lin, M.; Zhou, P.; Jiang, Y.F.; Zhou, F.C.; Lin, J.Y.; Wang, Z.J. Numerical investigation on comprehensive control system of cooling and heat insulation for high geothermal tunnel: A case study on the highway tunnel with the highest temperature in China. *Int. J. Therm. Sci.* **2022**, *173*, 107385. [CrossRef]
13. Zhang, H.; Hao, Z.H.; Zhang, G.; Tao, Y.C.; Wang, L. The cooling effect of high geothermal tunnel construction environment: A case of ice and spray method in an extra-long tunnel. *Int. J. Therm. Sci.* **2022**, *178*, 107606. [CrossRef]
14. Yuan, Q.; Peng, M.Q.; Yao, H.; Zhang, S.H.; Li, Y.L. The internal temperature field of shotcrete in high geothermal tunnel and its effect on microstructures and mechanical properties. *Constr. Build. Mater.* **2022**, *335*, 127507. [CrossRef]
15. Li, Z.G.; Wang, Y.; Tong, Y.P.; Zhang, S.H.; Niu, D.T. Compressive and hydration behavior of steel fiber-reinforced concrete under high geothermal environment. *Constr. Build. Mater.* **2023**, *406*, 133378. [CrossRef]
16. Chen, J.S.; Zeng, L.P.; Wang, W.; Qiao, M.; Zhao, S.; Zhu, B.S. Influence of main components of accelerators on mechanical property and hydration of Portland cement in a dry-hot geothermal environment. *Constr. Build. Mater.* **2023**, *394*, 132290. [CrossRef]
17. Cui, S.G.; Liu, P.; Su, J.; Cui, E.Q.; Guo, C.; Zhu, B. Experimental study on mechanical and microstructural properties of cement-based paste for shotcrete use in high-temperature geothermal environment. *Constr. Build. Mater.* **2018**, *174*, 603–612. [CrossRef]
18. He, S.L.; Cao, J.; Chai, J.R.; Yang, Y.; Li, M.; Qin, Y.; Xu, Z.G. Effect of temperature gradients on the microstructural characteristics and mechanical properties of concrete. *Cem. Concr. Res.* **2024**, *184*, 107608. [CrossRef]
19. Yan, B.Q.; Zhang, W.X.; Yi, W.J. Multi-scale study on the mechanical properties of concrete based on crack propagation under hygrothermal coupling. *J. Build. Eng.* **2024**, *91*, 109680. [CrossRef]
20. Zhou, Y.C.; Yan, Y.; Qin, Y.; Yu, C.; Wang, W.B.; Liu, J.P.; Wang, K.C. The effect of temperature rise inhibitor on the hydration and strength development of slag/fly ash blended cement paste. *Constr. Build. Mater.* **2023**, *395*, 132307. [CrossRef]
21. Li, M.; Xu, W.; Wang, Y.J.; Tian, Q.; Liu, J.P. Shrinkage crack inhibiting of cast in situ tunnel concrete by double regulation on temperature and deformation of concrete at early age. *Constr. Build. Mater.* **2020**, *240*, 117834. [CrossRef]
22. Li, Z.L.; An, R.; Zhang, W.Z.; Fan, X.; Jin, H.S.; Liu, J.; Liu, W.; Zhu, J.H.; Xing, F.; Jiang, Z.L. Investigating the effects of seawater and sea sand aggregates and supplementary cementitious materials on the early shrinkage and crack resistance of concrete. *Constr. Build. Mater.* **2023**, *392*, 131719. [CrossRef]
23. Liu, J.P.; Tian, Q.; Wang, Y.J.; Li, H.; Xu, W. Evaluation method and mitigation strategies for shrinkage cracking of modern concrete. *Engineering* **2021**, *7*, 348–357. [CrossRef]
24. Peng, Z.Z.; Wang, Q.; Zhou, W.; Chang, X.L.; Yue, Q.; Huang, C.B. Meso-scale simulation of thermal fracture in concrete based on the coupled thermal-mechanical phase-field model. *Constr. Build. Mater.* **2023**, *403*, 133095. [CrossRef]
25. Wang, Q.L.; Wang, M.N.; Yuan, Y.; Hu, Y.P.; Wang, H. Thermomechanical behavior of tunnel linings in the geothermal environment: Field tests and analytical study. *Tunn. Undergr. Space Technol.* **2023**, *137*, 105109. [CrossRef]

26. *GB/175-2023*; Ordinary Portland Cement. Ministry of Industry and Information Technology: Beijing, China, 2023. (In Chinese)
27. *GB/T 50081-2019*; Standard for Test Methods of Concrete Physical and Mechanical Properties. Ministry of Housing and Urban-Rural Development, People's Republic of China: Beijing, China, 2021. (In Chinese)
28. Fan, L.T.; Tao, L.L.; Duan, S.Q.; Luo, M.R.; He, C.; Zeng, Y.H.; Chen, Y.L.; Song, Y.; Qi, Z.F. Temperature field analysis in tunnel construction ventilation with emphasis on duct leakage and thermal conductivity. *Case Stud. Therm. Eng.* **2024**, *61*, 105102. [CrossRef]
29. Luo, M.R.; Zhang, X.Y.; Yuan, Z.B.; Wu, X.J.; Zeng, Y.H.; Ye, Y.Z. Thermal performance comparison and new layout scheme study of high geothermal tunnel insulation layer. *Case Stud. Therm. Eng.* **2023**, *52*, 103780. [CrossRef]
30. Cui, H.Z.; Li, Y.H.; Bao, X.H.; Tang, W.C.; Wang, S.Y.; Chen, X.S. Thermal performance and parameter study of steel fiber-reinforced concrete segment lining in energy subway tunnels. *Tunn. Undergr. Space Technol.* **2022**, *128*, 104647. [CrossRef]
31. Chen, Q.; Zhang, H.; Zhu, Y.M.; Chen, S.G.; Ran, G.Y. Study on distributions of airflow velocity and convective heat transfer coefficient characterizing duct ventilation in a construction tunnel. *Build. Environ.* **2021**, *188*, 107464. [CrossRef]
32. Lu, M.; Yu, L.; Wang, M.N.; Sun, B.L.; Zhou, Z.Y.; Tang, Y.H. A new approach in calculation of heat release during high geothermal tunnels construction considering ventilation time effect. *Int. J. Therm. Sci.* **2023**, *194*, 108589. [CrossRef]
33. Wang, G.F.; Fang, Y.Q.; Ren, K.F.; Deng, F.Y.; Wang, B.; Zhang, H. Prediction of the temperature field in a tunnel during construction based on airflow-surrounding rock heat transfer. *Buildings* **2024**, *14*, 2908. [CrossRef]
34. Wang, Y.; Zhou, X.H.; Liu, X.R.; Chen, X.; Xu, Q.; Wang, Q.L. Ambient temperature prediction model and cooling requirement analyze in the high-altitude construction tunnel passing through the abnormally high geothermal region. *Tunn. Undergr. Space Technol.* **2023**, *141*, 105360. [CrossRef]
35. Niu, D.T.; Zhang, S.H.; Wang, Y.; Hong, M.S.; Li, Z.G. Effect of temperature on the strength, hydration products and microstructure of shotcrete blended with supplementary cementitious materials. *Constr. Build. Mater.* **2020**, *264*, 120234. [CrossRef]
36. Liu, P.; Cui, S.G.; Li, Z.H.; Xu, X.F.; Guo, C. Influence of surrounding rock temperature on mechanical property and pore structure of concrete for shotcrete use in a hot-dry environment of high-temperature geothermal tunnel. *Constr. Build. Mater.* **2019**, *207*, 329–337. [CrossRef]
37. Shen, J.R.; Xu, Q.J.; Wang, S.G. Characterization of thermal damage and compressive strength during drying at elevated temperatures using ultrasonic pulse velocity. *J. Build. Eng.* **2023**, *75*, 107029. [CrossRef]
38. Hu, Y.P.; Wang, Q.L.; Wang, M.N.; Liu, D.G. A study on the thermo-mechanical properties of shotcrete structure in a tunnel, excavated in granite at nearly 90 °C temperature. *Tunn. Undergr. Space Technol.* **2021**, *110*, 103830. [CrossRef]
39. Chen, X.; Zhou, X.H.; Zhong, Z.L.; Liang, N.H.; Wang, Y.; Zhang, X.Y. Study on temperature field and influencing factors of the high geothermal tunnel with extra-long one-end construction ventilation. *Int. J. Therm. Sci.* **2023**, *191*, 108322. [CrossRef]
40. Luo, M.R.; Yuan, Z.B.; Fan, L.T.; Tao, L.L.; Zeng, Y.H.; Yan, Q.X. Investigating the coupling effect of ventilation and GHEs on temperature distribution and heat transfer characteristics. *Appl. Therm. Eng.* **2024**, *248*, 123211. [CrossRef]
41. *TB 10003-2016*; Code for Design of Railway Tunnel. National Railway Administration of People's Republic of China: Beijing, China, 2016. (In Chinese)
42. Ding, J.; Wang, X.; Sun, Z.; Liu, S.; Zhou, J.Y.; Wu, Z.S. Research on the cracking risk index of massive concrete based on Chemo-Thermo-Hygro-Mechanical multi-field coupling model. *J. Build. Eng.* **2024**, *98*, 111190. [CrossRef]
43. Zhou, X.H.; Chen, X.; Wang, Y.; Liang, N.H.; Liu, X.R. A method for predicting the ambient temperature distribution of high-temperature tunnels and influencing factors analyze. *Case Stud. Therm. Eng.* **2024**, *53*, 103831. [CrossRef]
44. Luo, M.R.; Tao, Y.C.; Yuan, Z.B.; Tao, L.L.; He, C.; Yuan, Y.P.; Tian, X.Y.; Zeng, Y.H. Effect of tunnel ventilation on surrounding rock temperature field and heat regulating circle during construction phase. *Tunn. Undergr. Space Technol.* **2024**, *150*, 105835. [CrossRef]
45. *Q/CR 9604-2015*; Technical Specification for Construction of High-Speed Railway Tunnel. China State Railway Group Co., Ltd.: Beijing, China, 2015. (In Chinese)
46. Guo, C.C.; Ji, X.Q.; Sun, H.; Qin, L.; Guan, H.; Chu, X.X. A theoretical model to predict the cooling effect of sprayed polymer under hydro-thermal condition. *Appl. Therm. Eng.* **2024**, *257*, 124166. [CrossRef]
47. Li, W.J.; Feng, Z.; Su, H.; Zou, S.H.; Zeng, L.P. Analysis of thermal insulation effect of off-wall insulation lining in high-temperature tunnel. *Case Stud. Therm. Eng.* **2024**, *61*, 104957. [CrossRef]
48. Wang, Y.; Zhou, X.H.; Liu, X.R.; Li, N.; Qi, Z.F.; Zhang, J.L. Investigation and optimization heat and humidity environmental control model in construction tunnels: A multifactorial approach incorporating ventilation parameters and hot water quantity. *Tunn. Undergr. Space Technol.* **2024**, *153*, 106039. [CrossRef]